EVALUATIONS OF THE STRONG GROUND MOTION PARAMETER BY EMPERICAL STOCHASTIC GREEN'S FUNCTION COMPUTING AND MICROTREMOR ARRAY MEASUREMENT AT PALU DEPRESSION AREA, CENTRAL SULAWESI, INDONESIA

Pyi Soe Thein[1], Subagyo Pramumijoyo[2], Kirbani Sri Brotopuspito[3], Junji Kiyono[4], Wahyu Wilopo[4] and Agung Setianto[6]

[1] *Geological Engineering Department, Gadjah Mada University*
[2] *Geological Engineering Department, Gadjah Mada University*
[3] *Physics Department, Gadjah Mada University*
[4] *Graduate School of Global Environmental Studies, Kyoto University*
[5] *Geological Engineering Department, Gadjah Mada University*
[6] *Geological Engineering Department, Gadjah Mada University*

**Corresspondence : pyisoethein@yahoo.com*

Abstract

In this study, we investigated evaluations of the strong ground motion parameter for Palu region. One of the major structures in Central Sulawesi is the Palu-Koro Fault system. Several powerful earthquakes have struck along the Palu-Koro Fault during recent years, one of the largest of which was an M 6.3 event that occurred on January 23, 2005 and caused several casualties. Following the event, we conducted a microtremor survey to estimate the shaking intensity distribution during the earthquake. From this survey we produced a map of the peak ground acceleration, velocity and displacement in Palu City. We performed single observations of microtremors at 151 sites in Palu City. The results enabled us to estimate the site-dependent shaking characteristics of earthquake ground motion. We also conducted 8-site microtremor array investigation to gain a representative determination of the soil condition of subsurface structures in Palu. . Four accelerometers were used in each array observation site. One was installed at a center of the circle with a radius, r. Other three were arranged on the circle with a shape of regular triangle. Observation duration time was 20～30 minutes and sampling frequency was 100 Hz. Sequential observations were conducted three times by changing the array radius; r=3, 10 and 30 meters. Then, a substructure profile was identified from the dispersion curve by using the Particle Swarm Optimization. From the dispersion curve of array observations, the central business district of Palu corresponds to relatively soil condition with Vs $\leq$ 300 m/s, the predominant periods due to horizontal vertical ratios (HVSRs) are in the range of 0.4 to 1.8 s and the resonant frequency are in the range of 0.7 to 3.3 Hz. Strong ground motions of the Palu area were predicted based on the empirical stochastic Green's function method. Peak ground acceleration and peak ground velocity becomes more than 400 gal and 30 kine in some areas and peak ground displacement becomes more than 17 cm in some areas, which causes severe damage for buildings in high probability.

Keywords: Palu-Koro Fault, Microtremor, Peak ground acceleration, Peak ground velocity, Peak ground displacement.

1. Introduction

Sulawesi Island, eastern Indonesia, is located at the junction between the converging Pacific-Philippine, Indo-Australian Plates and the Sundaland, i.e. the south-eastern part of the Eurasian Plate. The Central Sulawesi Fault System (CSFS), one of the major structures in SE Asia, cuts across Sulawesi Island from NW to SE, connecting the North Sulawesi subduction zone to the Banda Sea deformation zones.

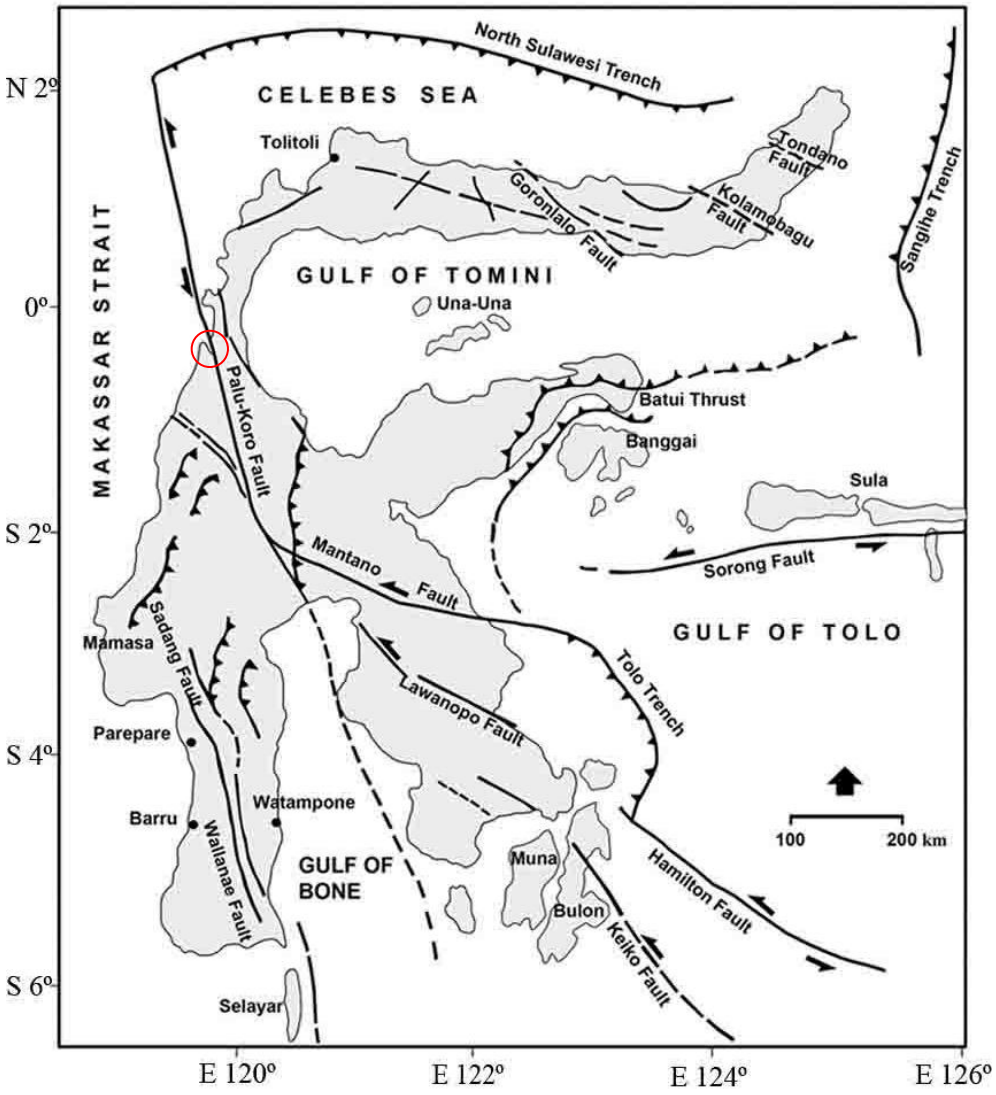

Figure 1 Tectonic map of Sulawesi [1]. Red circle: Palu depression area.

One of the major structures in Central Sulawesi is the Palu- Koro Fault system, which extends NNW- SSE direction and cross cuts Sulawesi along more than 300 km, from the North Sulawesi trench pass through Palu Bay, southward turn to the SE connect to the Matano and Lawanopo Faults and further eastward, both faults join to Tolo trench (Figure 1) [1]. In this study, Palu, where a large earthquake is expected in the near future, is considered to be a target area.

We carried out higher density single point observations and larger radius array observations. Based on the observed data, we calculated the distribution of the predominant and phase velocities of the Rayleigh wave.

2. Seismicity

Based on ISC catalog [2] more than hundred earthquakes with magnitude more than 6 were recorded in Sulawesi area. These earthquakes clustered at the northern arm of Sulawesi and along the Palu-Koro Fault System. Several earthquakes known along Palu-Koro Fault system such as Gimpu earthquake (1905), Kulawi earthquake (1907), Kantewu earthquake (1934), off shore Donggala earthquake (1968) which caused tsunami that destroyed 800 houses and killed 200 people at Donggala district. Considering the seismic activity along the Palu- Koro Fault system it should be significantly important to mitigate the natural hazard of Palu city area, especially on earthquake mitigation [3, 4].

Historical seismicity of Palu was reported since 19th century. Location of epicenters and level of intensity were still approximate based on the European resident note. The most important earthquakes that stroke Palu , are in 1927. These earthquakes caused 2,500 people died and 750 houses were severely damaged. These data show that Palu depression area is very vulnerable to earthquake disasters. Earthquake magnitude and depth and refers the sources (ISC) (Table 1). In Figure 2, the Yellow Circle indicates the most affected earthquake potentials can be expected within the radius of 200 km and the red circles indicate distribution of epicenters of the earthquakes with magnitude < 70 km, 70-300 km and > 300 km in depth. The projections in this figure are based on Digital Elevation Model from SRTM satellite image in 90 meter resolution. The variation in sizes of the circle suggests relative magnitude.

Table 1 Destructive earthquakes and earthquake-tsunami in the last 30 years in the Sulawesi region, Indonesia.(Source : http://earthquake.ISC)[2].

Date	Epicenter	Magnitude Richter Scale	Depth	Affected Area
1927	119.70 S;0.70 E	6.3		West Central Sulawesi
1967	19.40 S ; 3.30 E	6.3	20	Tinambung
1968	119.80 S; 0.70 E	7.4	25	West Central Sulawesi, Palu
1969	118.50 S; 3.10 E	6.1	13	South Sulawesi
1984	118.80 S; 2.77 E	6.6	14	Mamuju
1996	120.10 S; 0.83 E	7.7	15	Sulawesi, Palu
2005	121.11 S; 5.59 E	6.5	10	Sulawesi, Indonesia
2007	126.40 S; 1.22 E	7.5	22	Molucca Sea
2007	127.48S; 2.82 E	6.9	25	Molucca Sea
2008	122.10 S;1.29E	7.4	30	Halmahera, Indonesia
2011	122.81 S; 4.59E	6.2	9	Sulawesi,
2012	122.95 S; 3.26 E	4.6	539.1	Celebes Sea

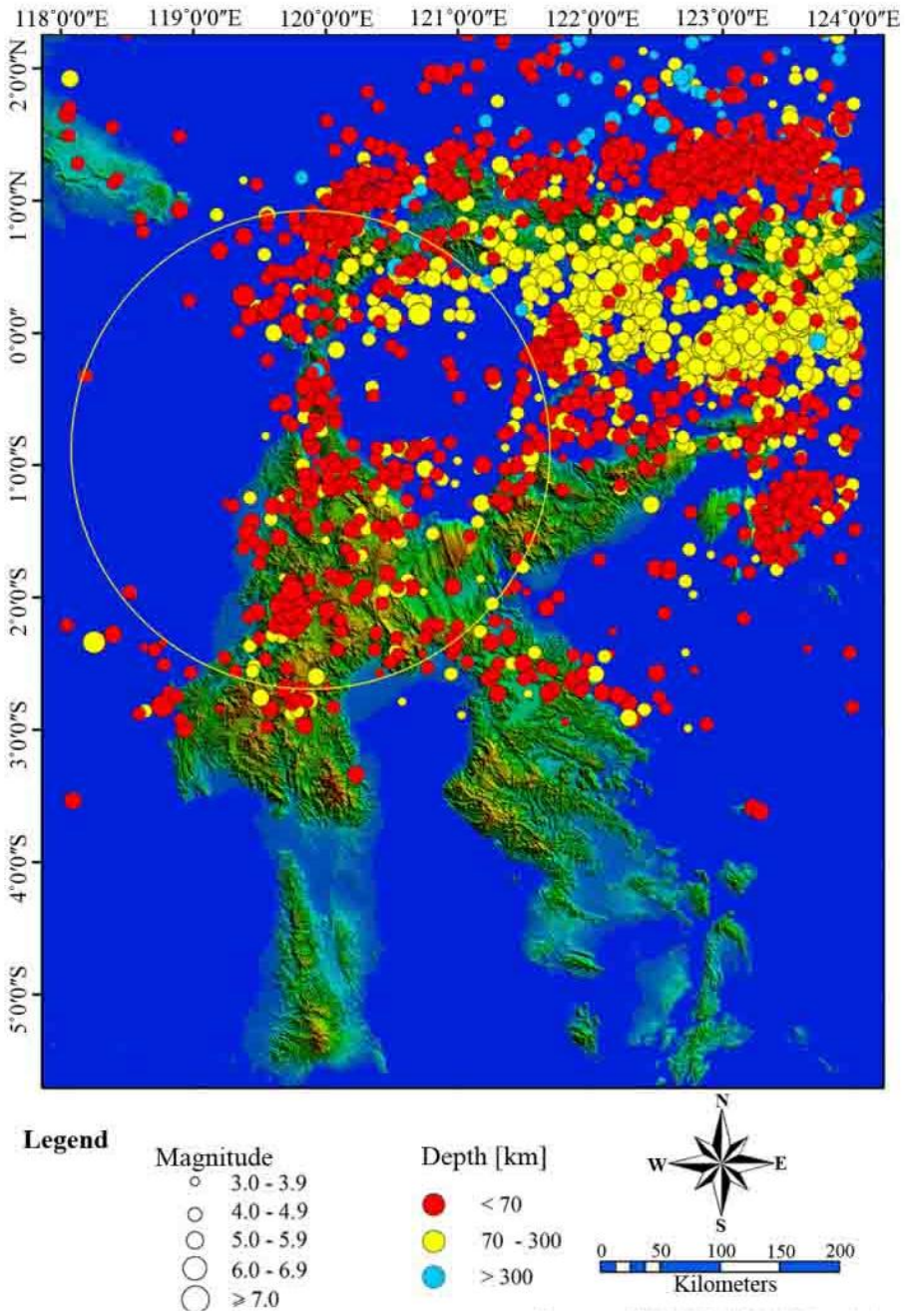

Figure 2 Epicentral distribution of some important earthquakes around Palu province [2]

3. Geometry of Palu Depression

Geometry of the Northern part of Palu-Koro fault system, shows a N-S trending asymmetric graben; including Palu Bay; and called as Palu depression, which is up to 7 km wide, 60 km long and bordered by steep triangular facets and truncated alluvial fans at West side, and gently step faults at East side. On both sides of the Palu depression can be observed the present of terraces up to 75 m above sea level [3]. To the South of Gumbasa this fault system is characterized by a narrow valley, segmented in average every 15 km with several

small depressions, i.e. Kulawi and Gimpu depressions. These depressions are interpreted as a result of pull-apart extension due to sinistral displacement of the fault. This sinistral displacement observed from offset of the rivers along the fault, i.e 100 - 600 m along the Palu-Koro fault and 200 - 600 m along the Matano fault [3, 4, 5, 6].

Figure 3 (a.) Three dimensional view of the Palu depression area

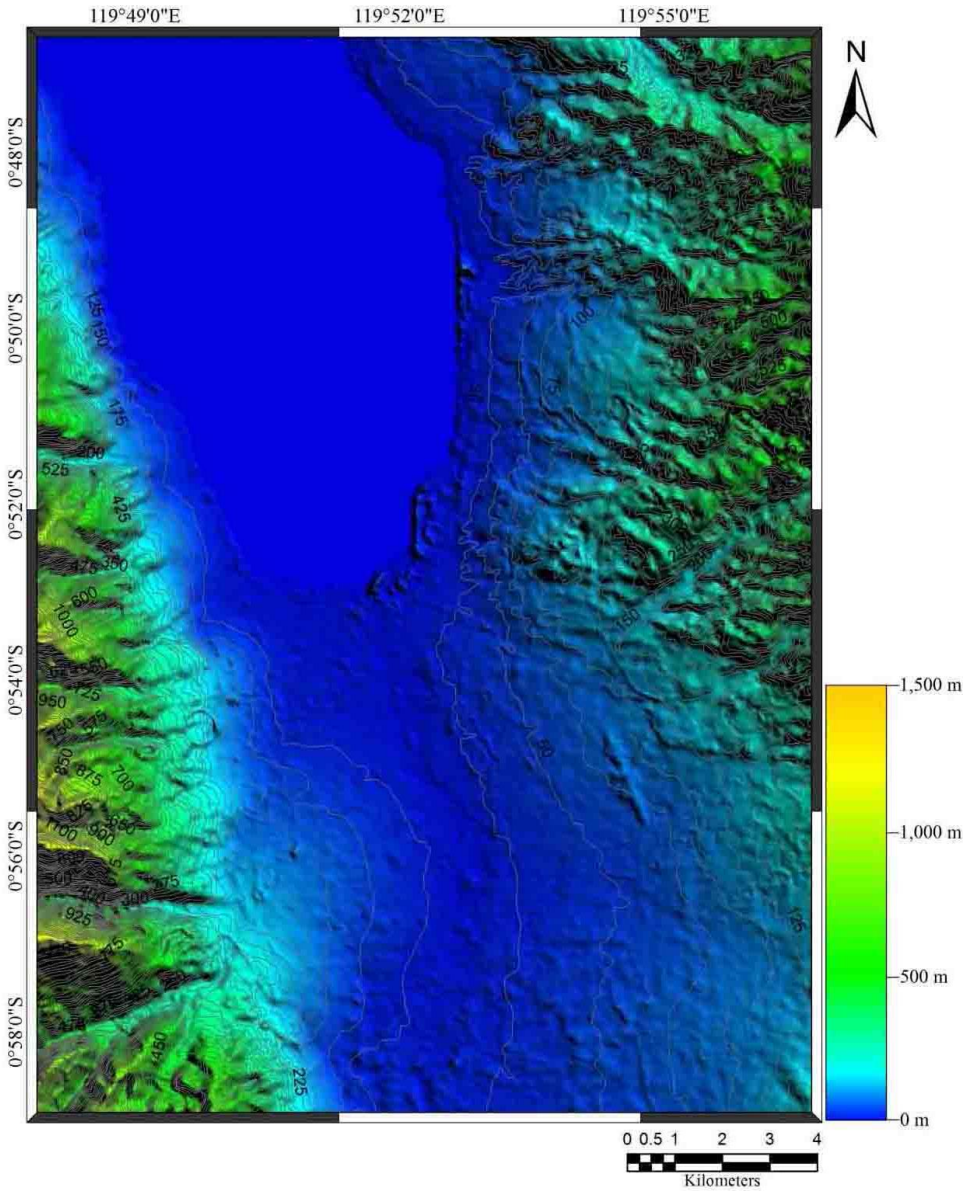

Figure 3 (b) DEM at Palu area

The topography of the Palu region in detail become firstly important to observe and to analyse (Figure 3 (a)). It can be combined topographic map, 1:50000 scale, and digital elevation model (DEM) from SRTM with 30 m resolution, to determine structural lineaments (Figure 3 (b)).

4. Geology of Palu Depression Area

Evolution of Neogene kinematics along the Palu-Koro fault was confirmed based on microtectonics approach, i.e.: sinistral strike-slip due to E-W compression, radial extensions caused by telescoping vertical movement of Neogene granitoid, and then left lateral with normal component displacement due to N-S extension/ E-W compression which is still active actually [7].

Palu depression area is filled by mostly clay, silt, and sand deposits as alluvial deposits (Figure 4), except on the border east or west consist of gravelly sands as colluvial wedges .The composition of gravel is granitic fragment to the northwest, mostly of schist on the west (Figure 5) and to the east the gravel consists of schist, igneous and sedimentary rocks. West escarpment to the north consists of granite (Figure 6) and granodiorite units, and to the south

consists of schist-phyllitic units. East escarpment consists of molasses [8]. Figure 7 shows geological map of Palu depression area.

Figure 4 Vertical position fossil fragment with alluvial deposits. (S 00°49.29.3' and E 119° 53.08.1')

Figure 5 Folded schist exposed on the west Palu (081298 and 9890521).

Figure 6 Igneous rock intruded in northwestern part of Palu (S 00°49.184' and E 119°47.526').

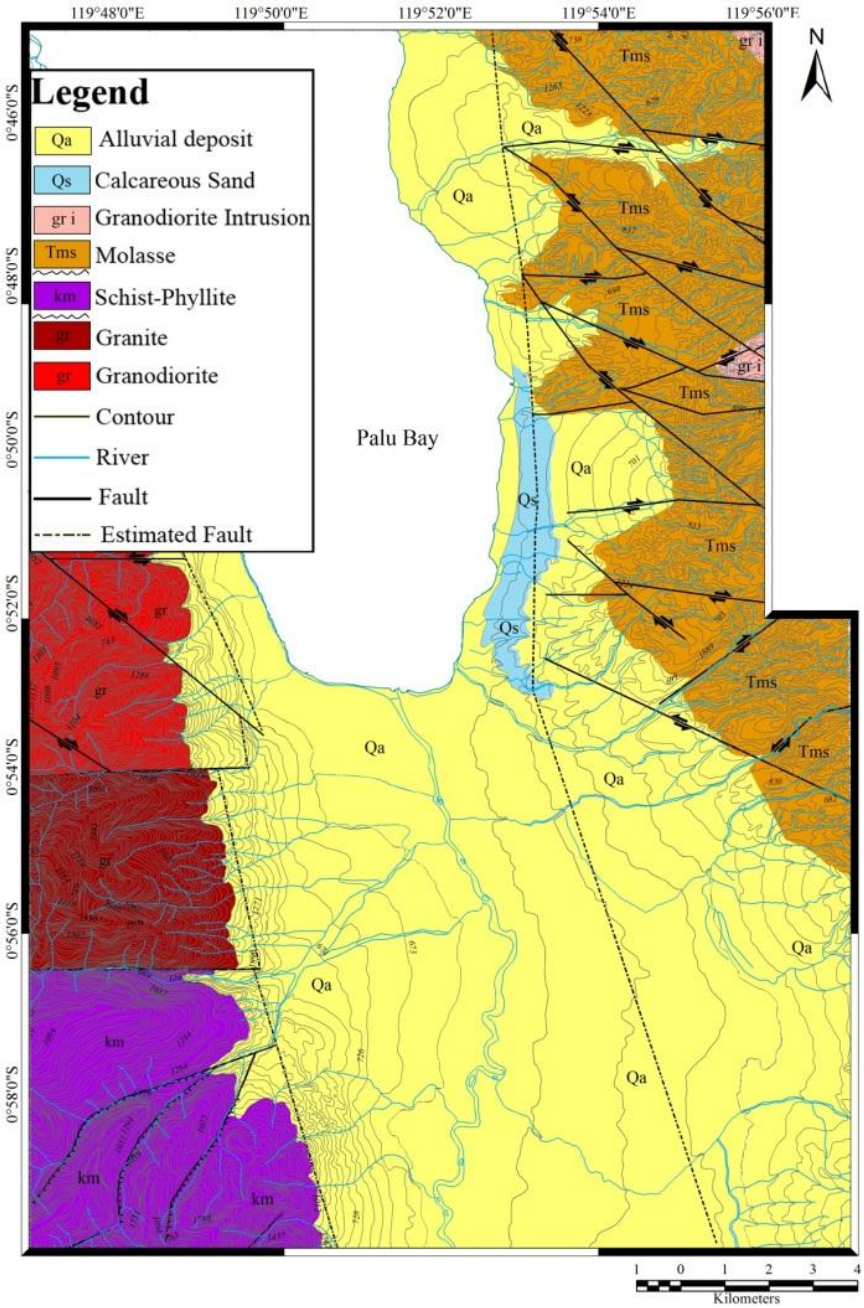

Figure 7 Geological map of Palu depression area "Indra, Ismawan, Ananda and Juwanto, 2012."

5. Observation Instruments

The instrument that used for microtremor measurements are primary instruments for this research. The instrument (shown in the following Figure 8) was used for the microtremor measurement of 8 points along the array observation lines.

Figure 8 Instrument of Network Senor Model VC-374 AVT.

The instrument shown in the Figure 9, model GPL 6A 3P that produced by Mitutoyo Corporation was also used for microtremor measurements in Palu City. All instruments have 3 sensors and measures for 3 direction; N-S, E-W and U-D.

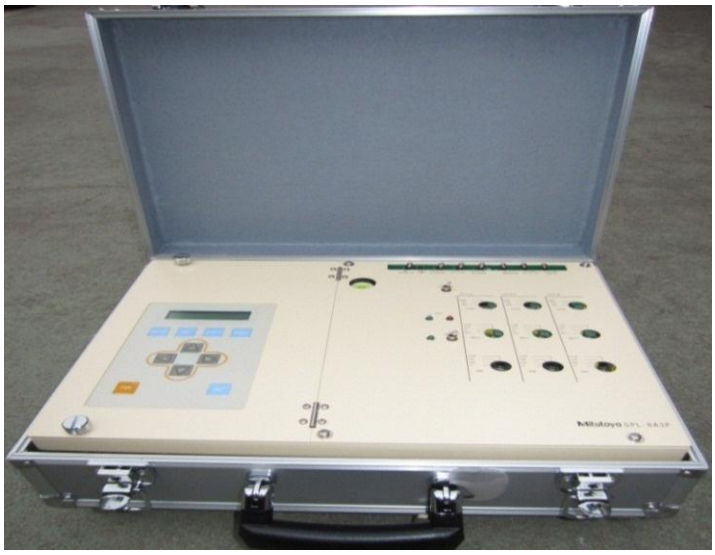

Figure 9 Instrument of Microtremor GPL- 6A3P Model, Mitutoyo Corporation.

6. Microtremor Single Station Observations

A three-component accelerometer with data logger, GPL-6A3P, produced by the Mitsutoyo Co. Ltd., was used. Observations were done in the daytime at places away from noises sources such as vehicle traffic and which provided stable conditions for the installed equipment such as a concrete or asphalt base. The number of single point observations was 151 (Figure 10). The sampling frequencies were 100 Hz or 500 Hz and the observation times were 10 to 15 minutes. Array observations were carried out at 8 sites with sampling frequencies of 100 Hz and observation times of 20 to 30 minutes.

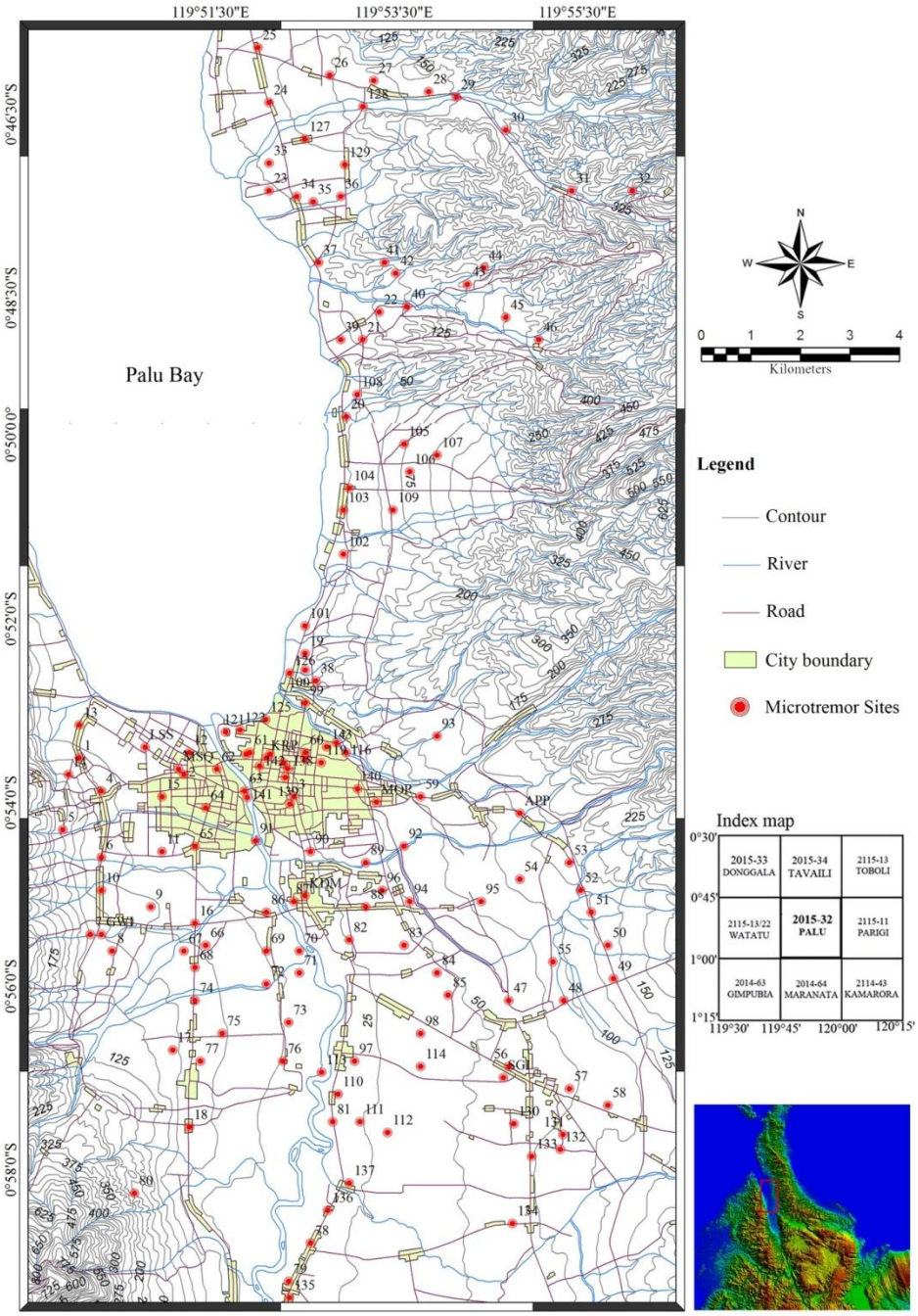

Figure 10 Location of the microtremor observation sites.

6.1 Analysis Method

The primary S-wave velocities structures are analyzed by H/V ratio and fundamental frequency from single station microtremor measurements. GPL-CG-Multi and GPL Communication Version 1.05 program operates on window 7. This program was developed using National instrument Lab View 5.1 and application builder. This program consists of displaying header information, data in a waveform graph and data in a table format (Figure 11).

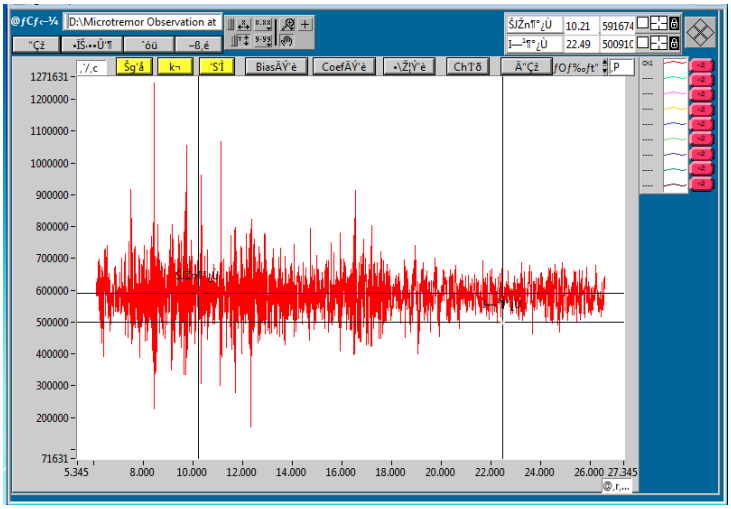

Figure 11 Measurment data file to convert a CSV data file format.

6.2 Predominant Period of H/V and Frequency

The spectral ratio of horizontal and vertical motion obtained by microtremor observations is called the H/V spectrum. The predominant period of an H/V spectrum is thought to be equivalent to the predominant period of the ground directly beneath the site. H/V spectra at each site in the target area were calculated. We classified the H/V spectra calculated into three types according to the shape of the spectra.

a. Type A: with short period peak (Figure 12(a))
b. Type B: with long period peak (Figure 12(b))
c. Type C: those without clear peaks

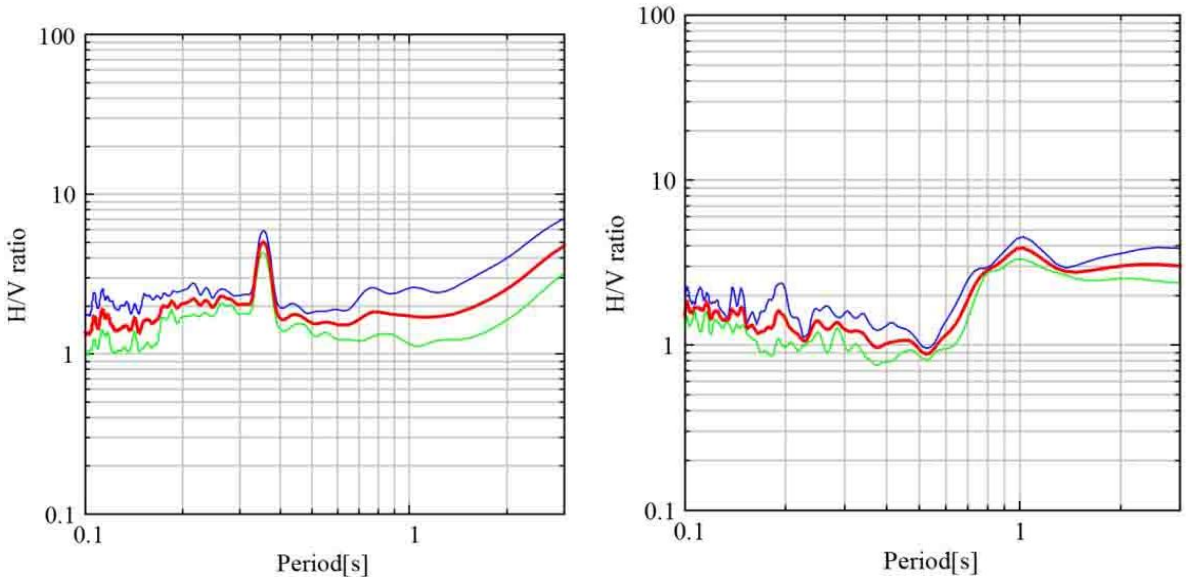

(a) short period peak (b) long period peak

Figure 12 Example of the H/V Spectrum ratio (a) short period peak and (b) long period peak (mean value and 1σ).

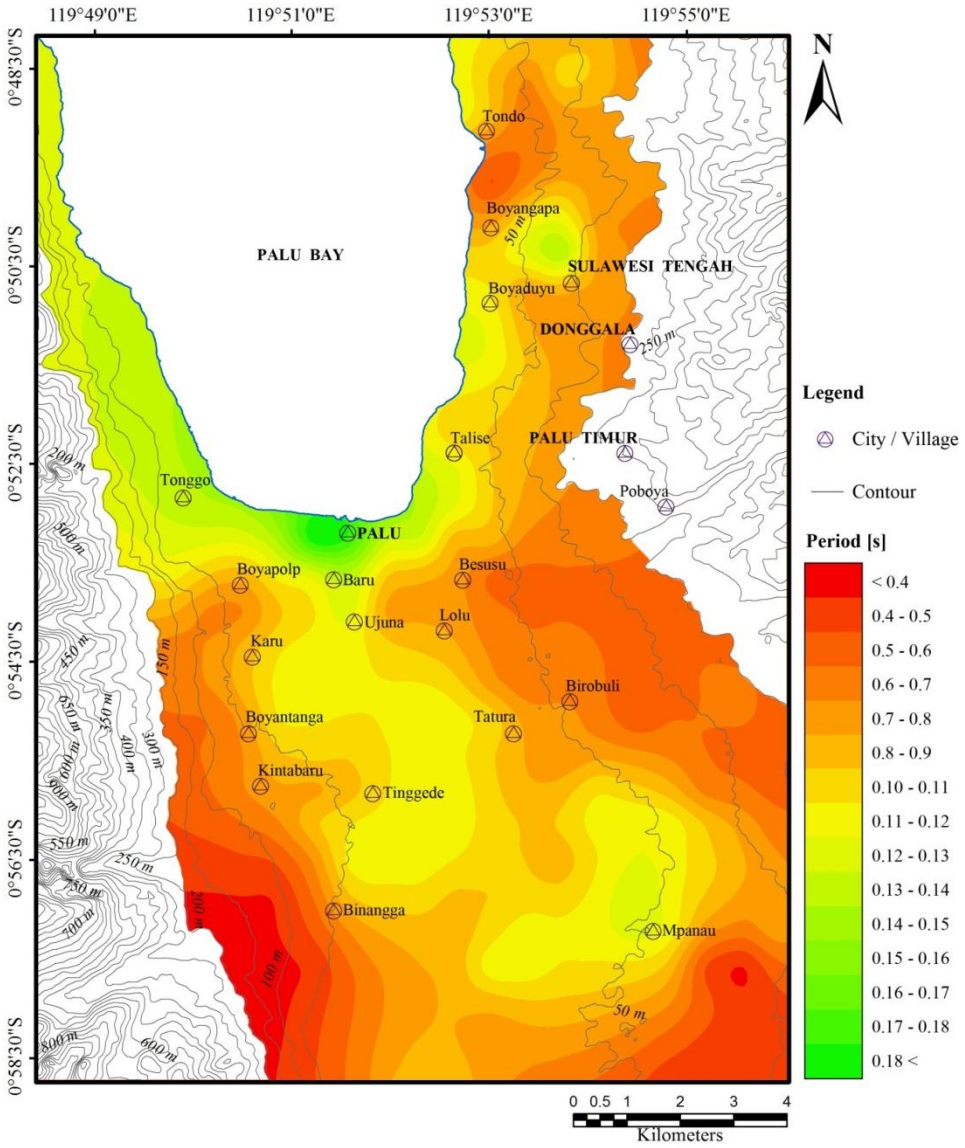

Figure 13 Spatial distributions of longer predominant period.

Equation (1) shows the method used to calculate HVSR using the observed records.

$$HVSR = \frac{\sqrt{(F_{NSi}(\omega))^2 + (F_{EWi}(\omega))^2}}{F_{UDi}(\omega)} \quad (1)$$

where, $F_{NSi}(\omega)$ and $F_{UDi}(\omega)$ denote the Fourier amplitude of the NS, EW and UD components of each interval, respectively, and (ω) is the frequency.

Distinct peaks express the characteristics of the layers for which the shear wave velocity is quite different. The shorter and longer periods are corresponding to a shallow and a deep soil layer. Type A and B reflect an effect of the shallow and the deep soil layer, respectively. Type C is an observation site that has hard soil. Thus, we established the data for both long and short predominant periods. Although the predominant period does not always indicate the characteristics of an individual layer because typically the actual shaking mode of the ground is complex, we assumed that the long and short periods reflected information from each layer. Although there are 151 observation points, the points are not adequate to cover all the target area. If each value of the predominant period obtained is considered to be a realization of a

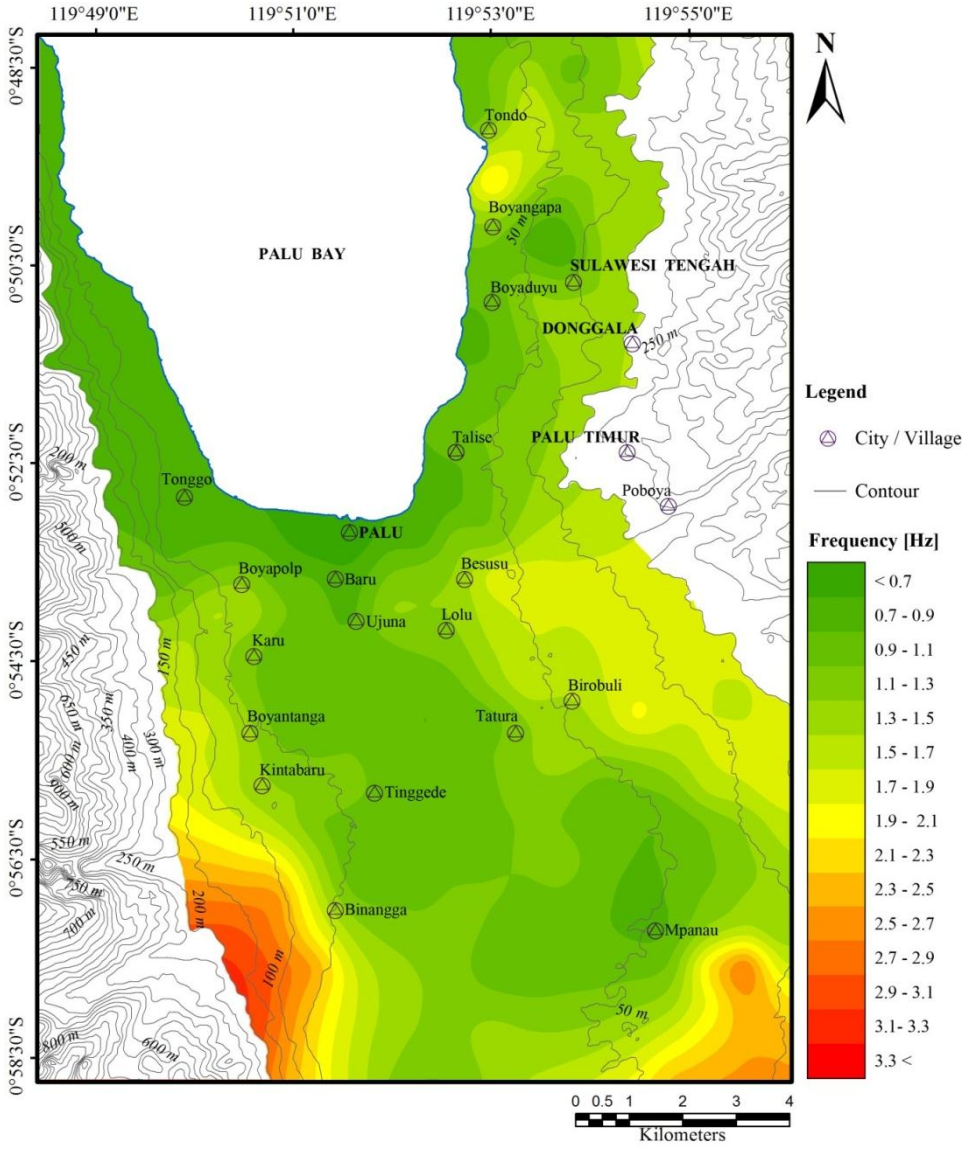

Figure 14 Map of frequency distribution for Palu City.

stochastic random field. Space interpolation is conducted by ordinary kriging technique [14]. The results are shown in Figure 13. The predominant periods of 1.0 - 1.8 seconds were on the alluvial fan area. The spatial correlations between predominant periods on the west side mountain, of which slope is steep, are shorter than those in the east side mountain and change more rapidly. The frequency distributions are in the range of 0.7 to 3.3 Hz (Figure 14).

7. Microtremor Array Observations

7.1 Spatial Autocorrelation (SPAC) Method

Aki (1957) [9] has introduced the correlation method to estimate the phase velocity by having an array of receivers equally spaced on a circle of radius *r* and having an extra receiver at the center as shown in Figure 15. Using a Fourier transform, observation records at receiver A and B can be expressed as follows [10]:

$$X_A(f) = U_A(f)\exp(-i\phi_A(f)) \quad (2)$$

$$X_B(f) = U_B(f)\exp(-i\phi_B(f)) \quad (3)$$

where, f indicates frequency, i is imaginary number, U, ϕ denote amplitude and phase, respectively,suffixes denote observation points. The coherence between receiver A and B can be expressed as following:

$$coh(f,r) = \frac{X_A(f)\cdot X_B^*(f)}{U_A(f)\cdot U_B(f)} = \exp\{i(\phi_B - \phi_A)\} = \exp\left\{i\frac{2\pi fr}{c(f,\psi)}\right\} \quad (4)$$

where, the superscript "*" denotes complex conjugate, ψ indicates azimuth angle between incoming wave and the line that links the point A and B, c denotes apparent phase velocity. However, in practice, we do not know arrival direction of incoming wave before a data processing. In order to solve directional dependency, the coherence between each of the receivers on the circle and the one in the center are averaged to obtain the SPAC coefficient, ρ, which is related to the function:

$$\rho(f,r) = \frac{1}{2\pi}\int_0^{2\pi}\exp\left\{i\frac{2\pi fr}{c(f,\psi)}\right\}d\psi = J_0\left(\frac{2\pi fr}{c(f)}\right) \quad (5)$$

where, $J_0(\cdot)$ stands for the zeroth-order Bessel Functions of the first kind. Once the SPAC coefficient is obtained from observation data, the phase velocity, c, can be determined by fitting the function appearing on the right-hand side of eq. (5) for each frequency, f.

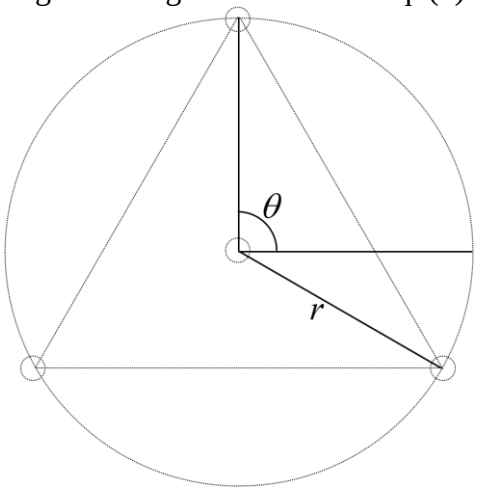

Figure 15 Configuration of a four point triangular array.

7.2 Dispersion Curve by Array Observations

The velocity of surface wave is well known to vary as a function of frequency (or period) due to dispersive characteristics [10, 11]. Therefore, the substructure can be estimated from observed dispersion curve. We carried out array observations at eight sites in Palu (Figure 16). Dispersion curves were calculated using the SPAC method. Four accelerometers were used in each array observation site. One was installed at a center of the circle with a radius, r. Other three were arranged on the circle with a shape of regular triangle. Observation duration time was 20～30 minutes and sampling frequency was 100Hz. Sequential observations were conducted three times by changing the array radius; r=3, 10 and 30 meters. Then, a substructure profile was identified from the dispersion curve by using the Particle Swarm Optimization (Keneddy. J., 1995; Noguchi, T. et al., 2009) [12,13].

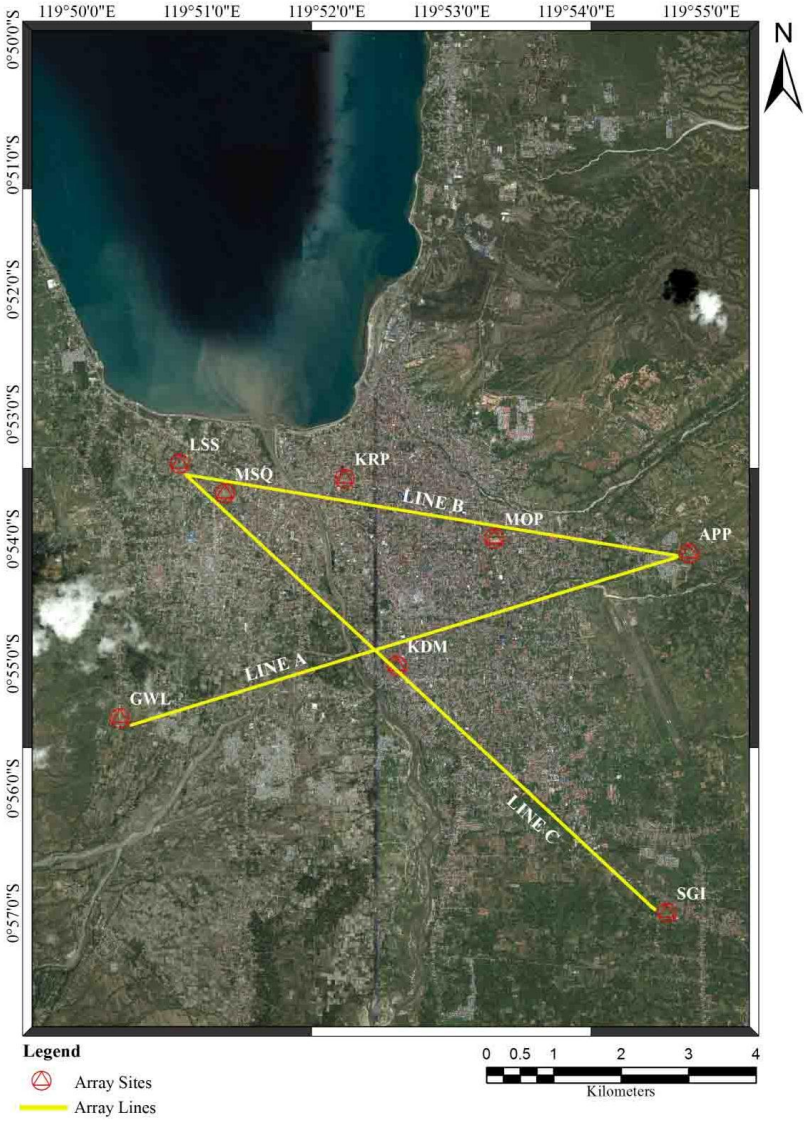

Figure16 Three survey lines for array observation (Line A, Line B, and Line C)

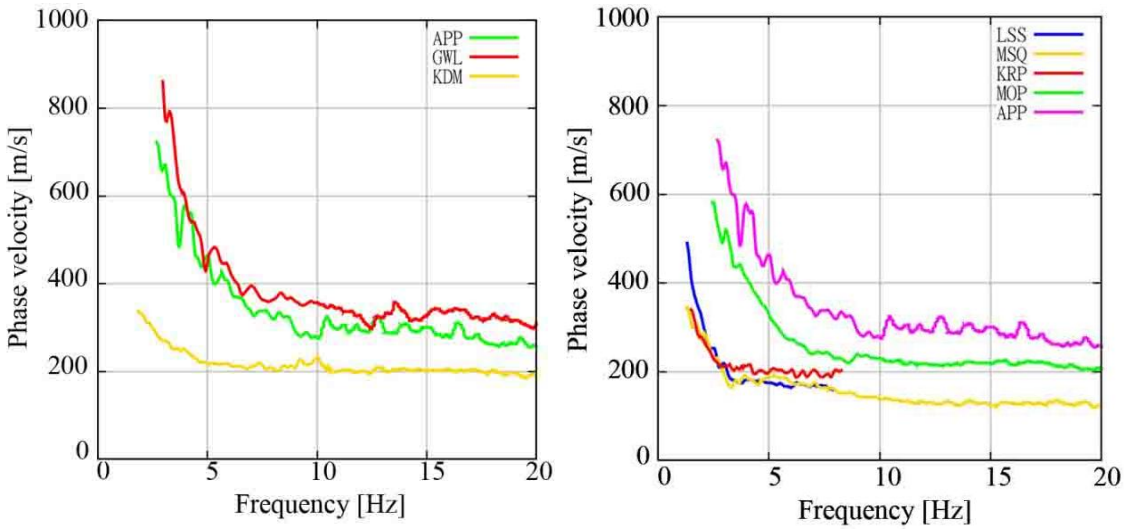

(a) Line A (b) Line B

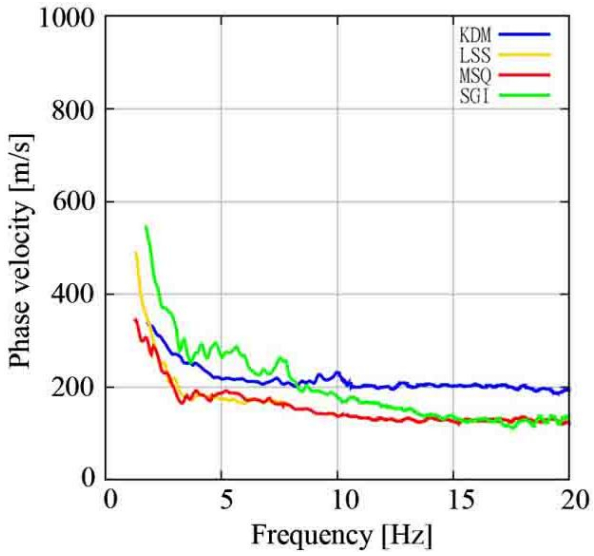

(c) Line C

Figure17 Dispersion curves obtained for each survey line (a) Line A, (b) Line B and (c) Line C.

The dispersion curves obtained are shown in Figure 17 (a), (b) and (c) for each survey. For line A, the phase velocity corresponding to shallow ground with a high frequency range is about 369 m/s at APP, about 423 m/s at GWL, about 318 m/s at KDM, about 318 m/s at KRP, about 279 m/s at LSS, about 348 m/s at MOP, about 285 m/s at MSQ and about 317 m/s at SGI. The soft ground extended beneath LSS, which is the nearest site to the coast. The ground beneath the sites higher than GWL has relatively hard surface soil compared with the plain along the coast. Since the minimum phase velocity in the high frequency range is around 300 m/s, the soil profile is very similar along line B and line C. The dispersion curves obtained here had no discrepancies in the distribution of topography, altitude and predominant period. We could estimate subsurface sedimentary layers in the plains using these dispersion curves.

8. Estimation of Vs Structures and Inversion

8.1 Application of PSO

By conducting an inversion analysis using the Particle Swarm Optimization (PSO) algorithm on the above dispersion curves, the subsurface structure beneath the site can be estimated. The PSO is a solution method for a non-linear optimization problem [12]. We estimate the subsurface structure of the model by minimizing the difference between the observed and theoretical phase velocity curves.

$$\mathrm{F} = \sum_{i=1}^{N} w_i \sqrt{(c_i^0)^2 - (c_i^T)^2} \qquad (6)$$

where F is an objective function that should be minimized, c_i^0 and c_i^T are the observed and theoretical phase velocities, and w_i is a weighting function. c_i^0 and c_i^T are given in discretized frequency (i=1,2,…,N). The PSO uses a particle swarm that has information about position and velocity. The particle swarm moves around the space with updating information and settles at the optimized point. During the optimization, the particle swarm has a best solution for both the group (g-best) and individual (p-best) in every step. The basic procedure of PSO is as follows. After setting the initial values of the number of particles and

iterations, an initial position and velocity are given to x_d^k and v_d^k, in which d is a particle number. The value of the objective function is calculated for each particle. The best solutions for the particle, *d*, and for the group, g, at k-th iteration are defined as p_d^k and p_g^k. The the position and velocity are updated as

$$v_d^{k+1} = wv_d^k + c_1 r_1 \left(p_d^k - x_d^k\right) + c_2 r_2 \left(p_g^k - x_d^k\right) \quad (7)$$

$$x_d^{k+1} = x_d^k + v_d^{k+1} \quad (8)$$

where r_1 and r_2 are random values with the range of [0,1], c1 and c2 are constants, and w is the inertia weighting. This process is repeated as k=k+1 until the number of iterations exceed a setting value.

Before performing the inversion analysis, the subsurface structure was assumed to consist of horizontal layers of elastic and homogeneous medium a semi-infinite elastic body. The shear wave velocity and thickness of each layer are the parameters that were determined by inversion analysis. The results obtained enable us to determine the soil condition of the subsurface structure [14]. Figure 18 shows Vs structures of the ground along the survey lines (a) Line A, (b) Line B and (c) Line C.

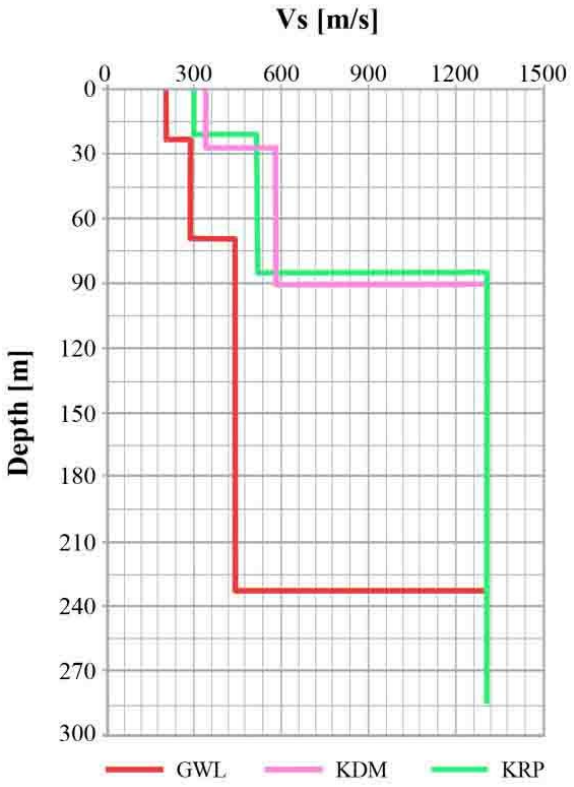

(a) Line A

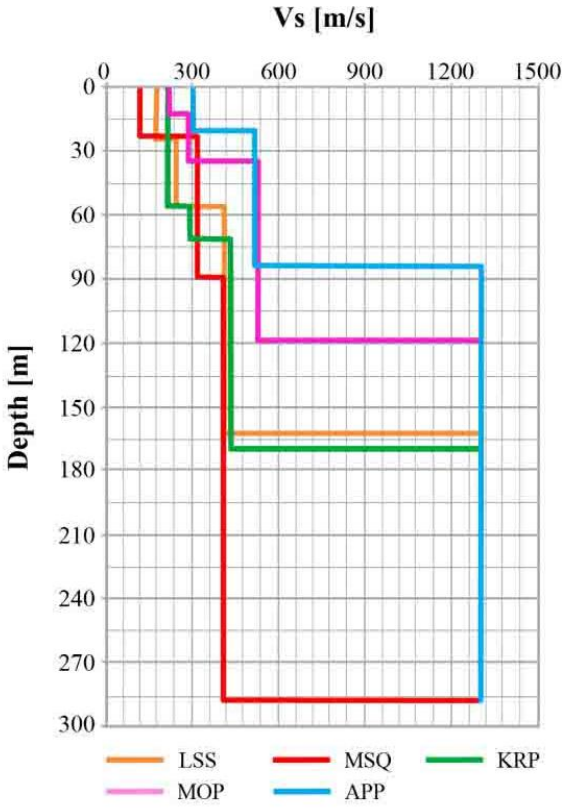

(b) Line B

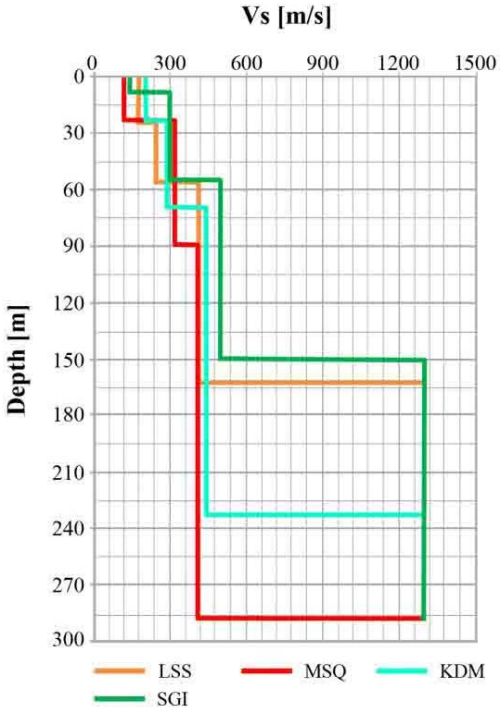

(b) Line C

Figure 18 Vs structures of the ground along the survey lines (a) Line A, (b) Line B and (c) Line C

❾. Inversion

The identified soil parameters by the inversion at MSQ are shown in Table 2. Figure 19 shows dispersion curve of the ground along the survey lines, respectively.

Table 2 Identified ground parameters at MSQ

Layer	ρ [t/m3]	*Vp*[m/s]	*Vs*[m/s]	*H* [m]
1	1.7	798	124	22
2	1.8	1,303	319	66
3	1.9	1,496	413	198

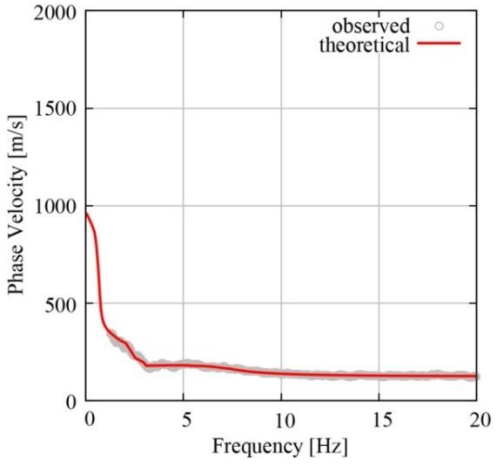

Figure 19 Dispersion curve at MSQ

10. Modeling Of Subsurface Soil Structure In Palu

We could obtain Vs structures at array observation sites, however, the ground profiles are not uniquely determined.

In this study, we proposed simple two layer model in Palu by averaging the first three layers of all array sites. Shear wave velocity of the first layer modeled is 300m/sec. By combining with the first peak of *H/V* data, we can obtain the thickness of the first layer. The technique used was the 1/4 wavelength principle, which can approximately be extended to multi layered media.

$$T = 4H/VS \qquad (9)$$

where, *H* is a thickness of a layer, *Vs* shear wave velocity and *T* predominant period. Figure 20 shows two dimensional model of the subsurface soil structure at Palu city (a) Line A, (b) Line B and (c) Line C. Figure 21 shows three dimensional shape of the estimated subsurface soil structure. The distribution of thickness for the first layer of which *Vs* is ≤ 300m/sec in Palu area is shown in Figure 22, in which the rapidly varying area of the subsurface condition and dense observation area are enclosed.

The shear wave velocities, V_s^* of layers are calculated by the weighted average, for which the weight is the reciprocal of square of distance from the array observation points, APP, GWL, KDM, LSS, MOP, MSQ and SGI, as

$$V_s^* = \frac{\Sigma \frac{V_{Si}}{x_i^2}}{\Sigma \frac{1}{x_i^2}} \qquad (10)$$

where i defines the array sites (i-1,2,..7),and x_i indicates the distance between an array observation site and the center of the mesh.

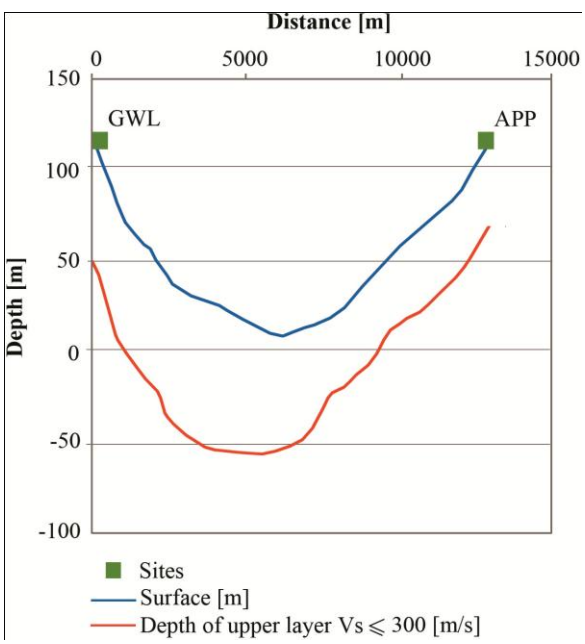

(a)

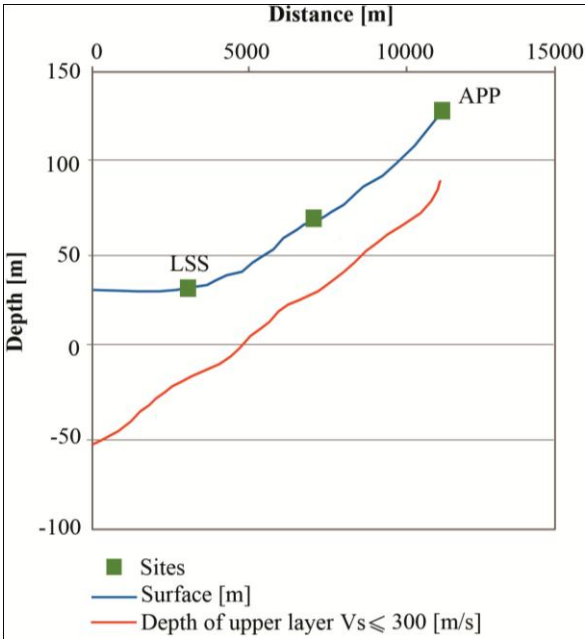

(b)

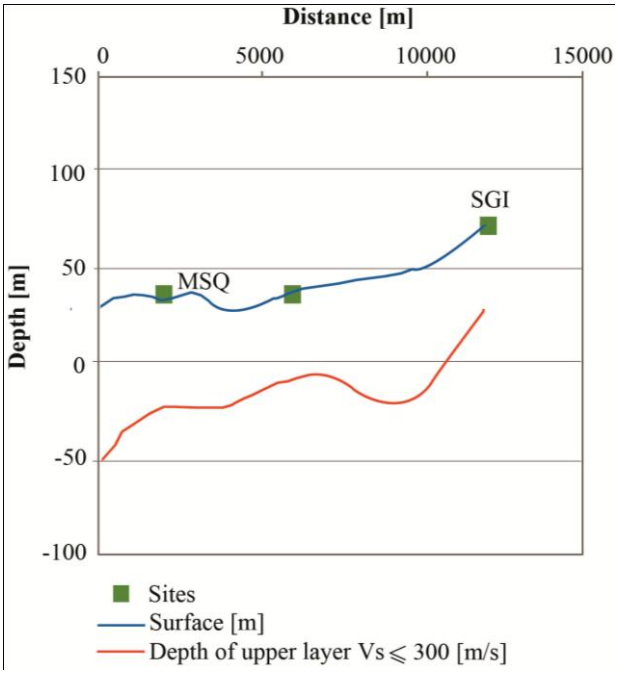

(c)

Figure 20 Two dimensional model of the subsurface soil structure at Palu city (a) Line A, (b) Line B and (c) Line C.

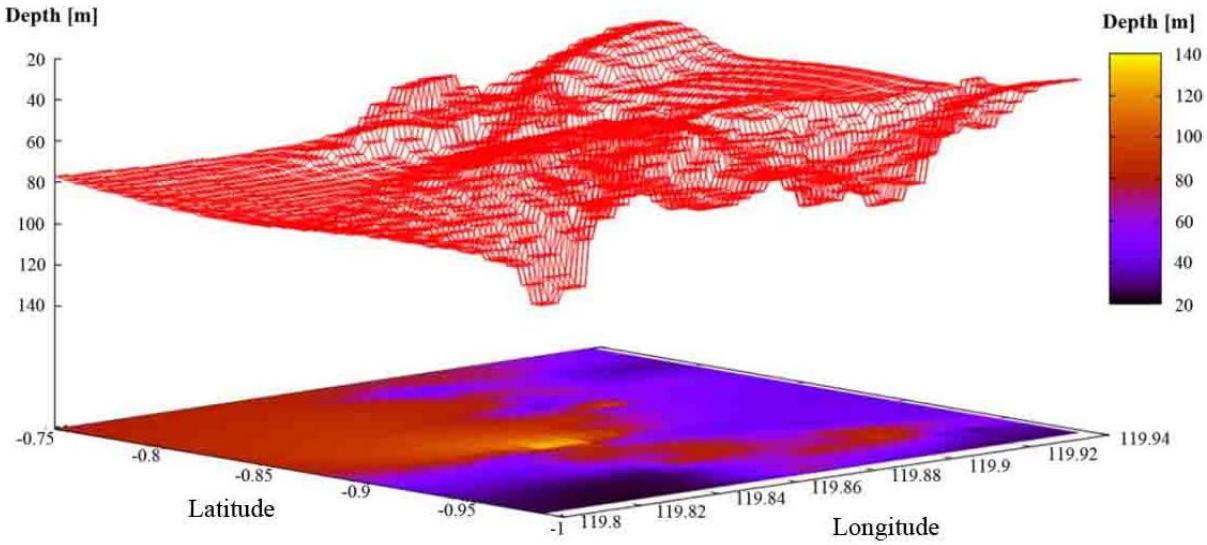

Figure 21 Three dimensional shape of the estimated subsurface soil structure.

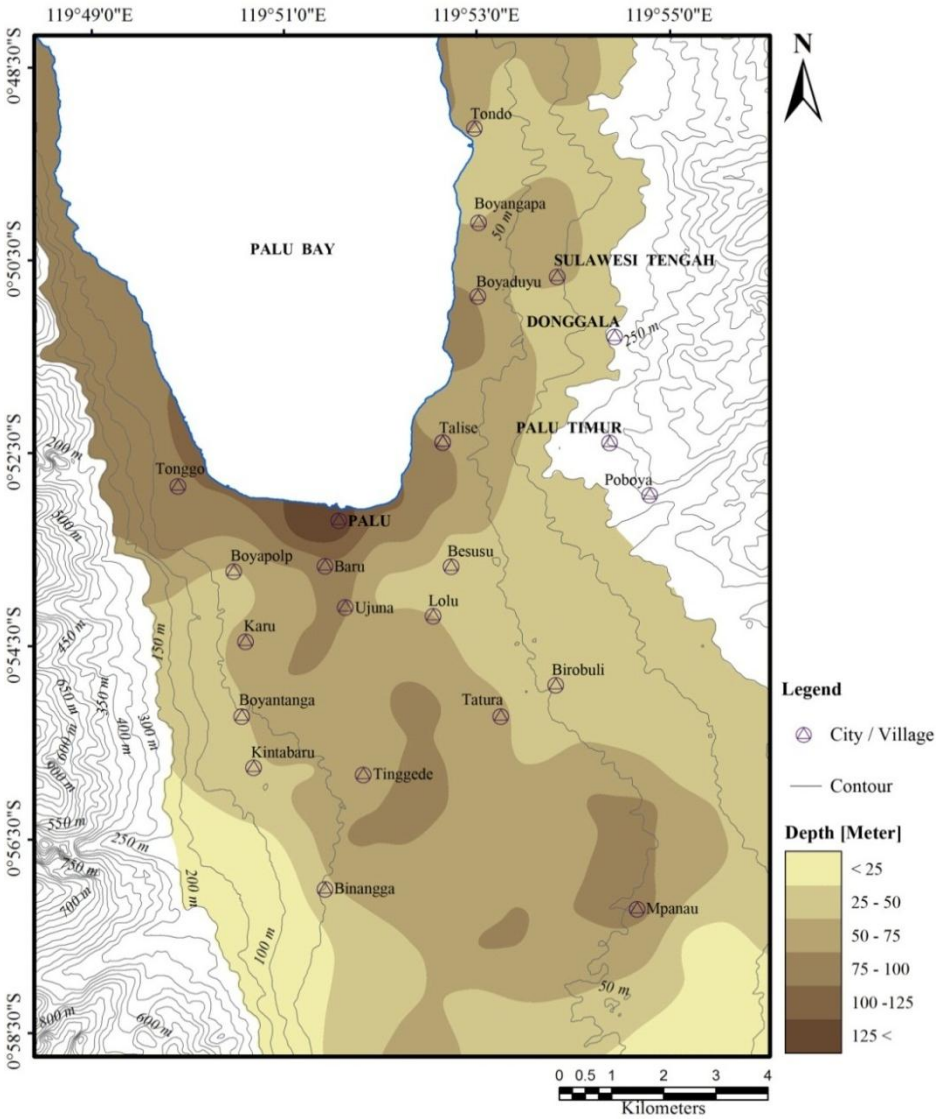

Figure 22 Depth of the engineering bed rock.

11. Strong Ground Motion

Strong ground motions of the Palu area were predicted based on the stochastic Green's function method (Figure 23).

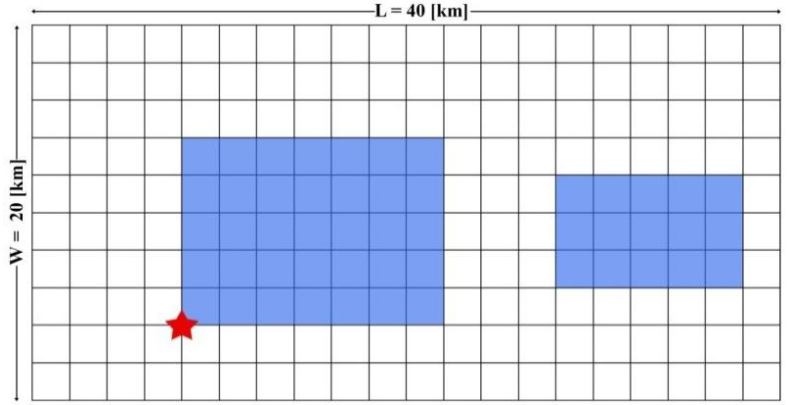

Figure 23. (a) Fault model of the 2005 Palu, Indonesia earthquake. Star indicates the rupture starting point. (b) characterized source model for the 2005 Palu earthquake. Rectangular regions with the blue colours show the area of the asperities. Star indicates the rupture starting point.

Table 3 Macroscopic source parameters

Latitude（°）	119.933°E	Fault area（km^2）	800
Longitude（°）	-1.198°S	Shear wave velocity （km/s）	3
Top depth d（km）	0	Mean density ρ(t/m^3）	2.4
Bottom depth（km）	20	Modulus of rigidityμ（N/m^2）	2.16E+10
Length L（km）	40	Average slip（m）	0.21
Width W (km）	20	rupture velocity V_r （km/s）	3
Strike（°）	342.1°	High-frequency limit (Hz)	10
Slope（°）	90		
Slip angle（°）	0°		
Moment magnitude	Mw=6.3		

Table 4 Microscopic source internal parameters

Asperities such as internal parameters	
Total area of asperity S_a (km^2)	200
Average slip D_a of asperity in (m)	0.20
Total amount M_oa moment in asperity (dyn· m)	3.55E+25
Total stress parameters Δσ_a of asperities (MPa)	3.82
Asperity 1	
S_a1 total area of one asperity (km^2)	140
Average slip D_a1 of asperity 1 in (m)	0.41
Total amount M_oa1 moment in asperity 1 (dyn · m)	5.98E+22
Total stress parameters Δσ_a1 one asperity (MPa)	21.82
Rise time (s)	2.1
Asperities 2	
Total area of asperities S_a2 2 (km^2)	60
Average slip D_a2 of asperity 2 in (m)	0.41
Total amount M_oa2 moment in asperity 2 (dyn · m)	9.18E+22
Total stress parameters Δσ_a2 of asperity 2 (MPa)	50.93
Rise time (s)	1.26
Background area	
Area S_b (km^2)	600
Slip D_b (m)	0.22
Seismic moment M_ob (dyn · m)	1.55E+22
Stress parameters Δσ_b (MPa)	9.2
Rise time (s)	4.20

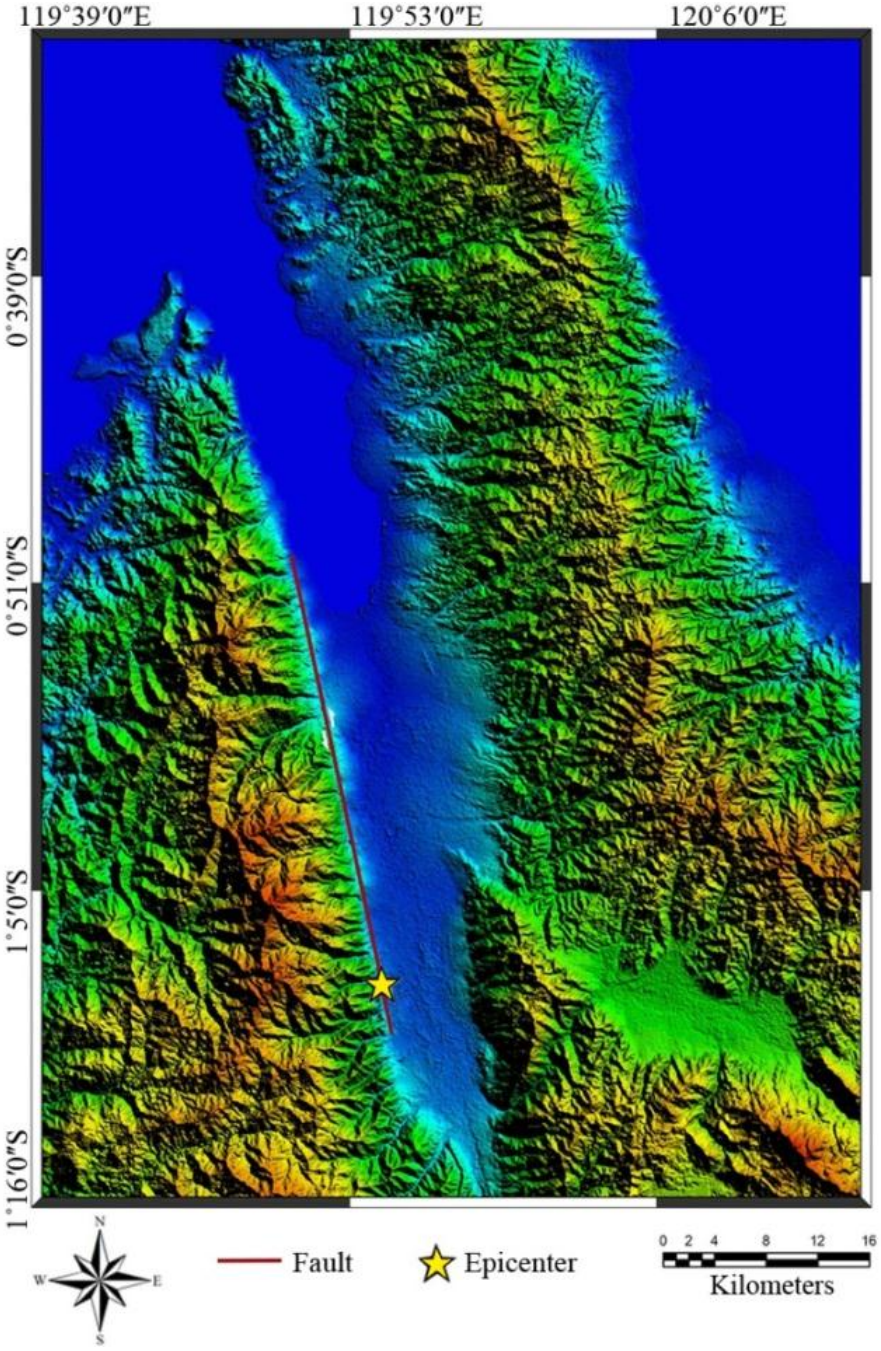

Figure 24 the location of the fault and epicenter.

In this study, ground model is constructed by combining two layer model and average seismic bed rock model used in Japan, because there is no bed rock information in this area (Table 3 and 4). The fault model referred is an earthquake with moment magnitude of 6.3 on 23 January 2005 in Palu, Indonesia, of which epicenter was latitude 119.933 and longitude -1.198. Figure 24 shows the location of the fault and epicenter.

12. Strong Ground Motion Parameters

12.1.Peak Ground Acceleration And Velocity

Distribution of the estimated peak ground accelerations and peak ground velocities are shown in Figure 25 and 26. The component of the shaking is NS. There are high accelerations and velocities are as appears along the fault, especially near the epicenter. There occurred relatively large shaking at the mouth of Palu river because of the deeper thickness of the

sediment. Peak acceleration becomes more than 400 gal in some areas, which causes severe damage for buildings in high probability. To prevent severe damage, firstly we have to check the vulnerability of the building in Palu, and if necessary, we have to take a countermeasure for strengthening of the structures. This is the first trial to estimate the shaking and the damage under the condition of the occurrence of a future Palu-Koro earthquake. We accumulate detailed information about not only the ground but also the inventory for disaster mitigation in Palu.

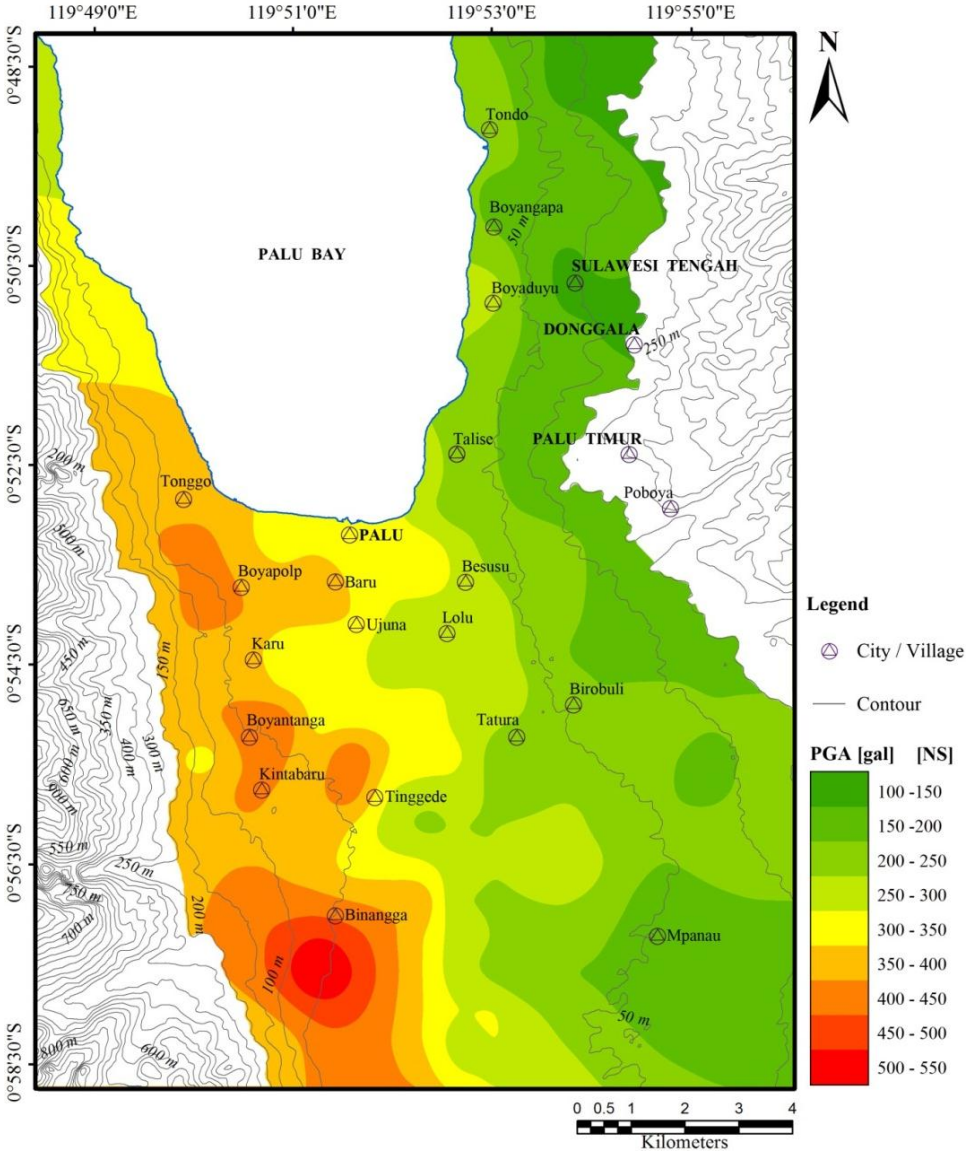

Figure 25 Peak ground acceleration [NS] map on Palu area.

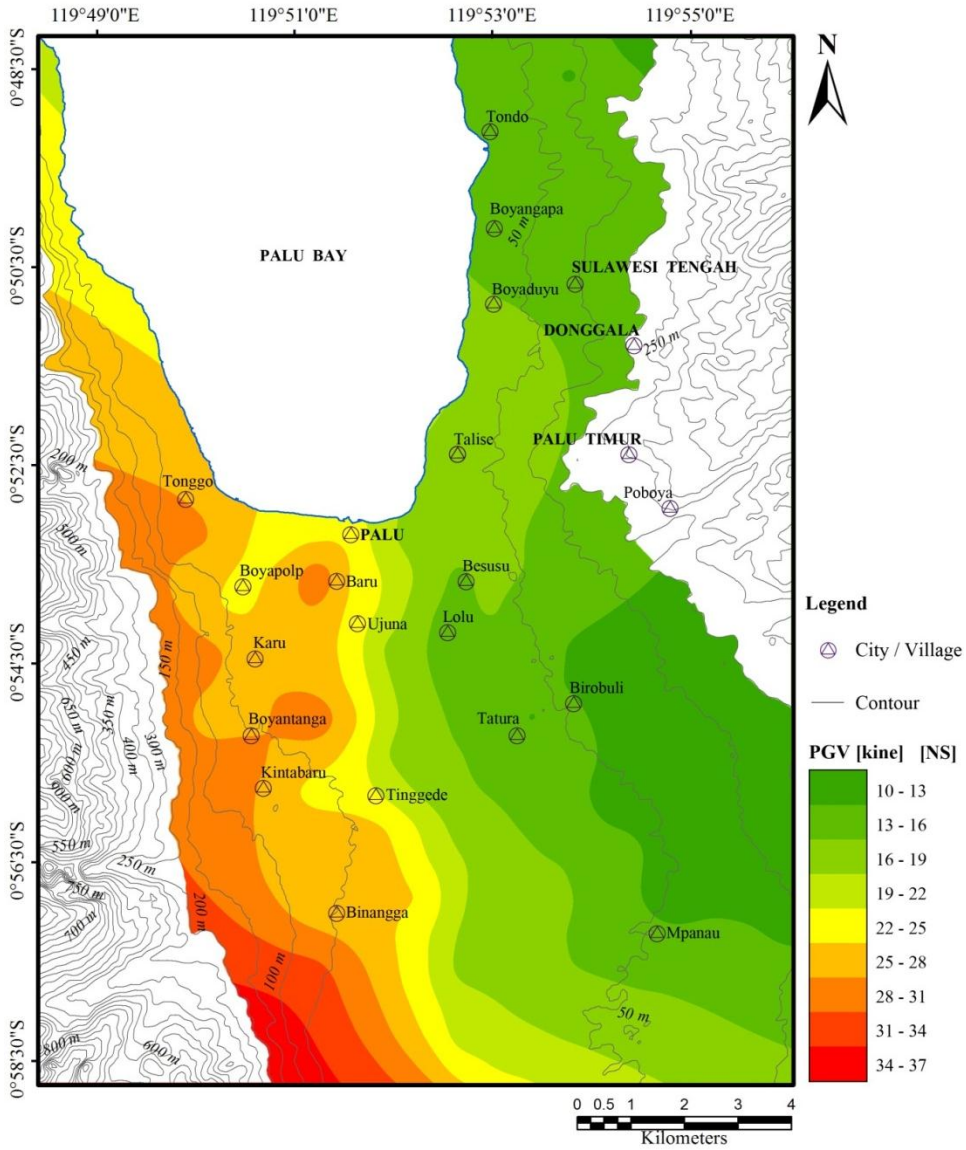

Figure 26 Peak ground velocity [NS] map on Palu area.

12.2. Peak Ground Displacement (PGD)

The peak ground displacement (PGD) map is produced from displacement time history output of response analysis where synthetic wave forms of 2005, Palu earthquake is used as input bedrock motion. As shown in Figure 27, southern part of the area, especially along Palu-Koro fault shows highest displacement zones.

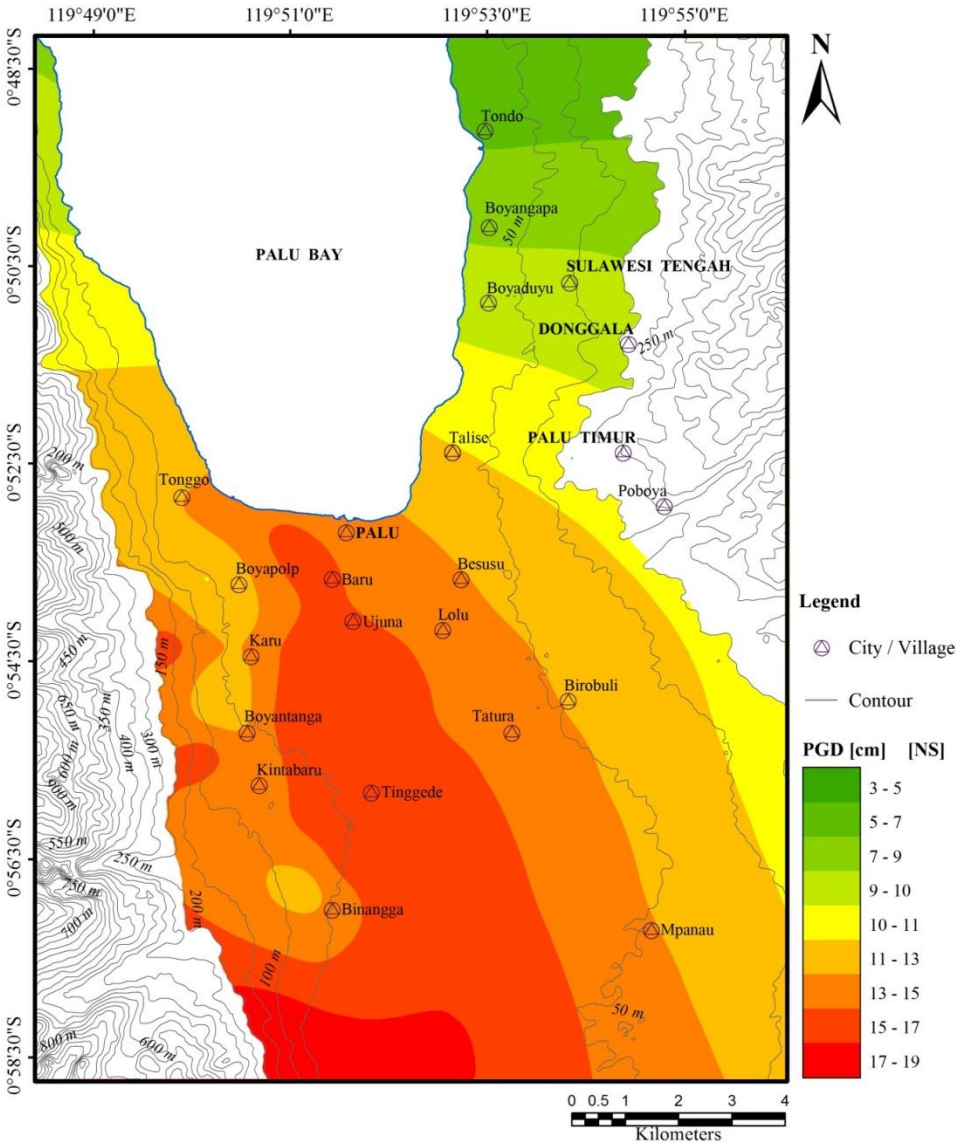

Figure 27 Peak ground displacement [NS] map on Palu area.

13. Conclusions

Our observations and analyses provide useful and practical data for earthquake disaster mitigation in Palu. The procedure employed and conclusions obtained in this study are as follows.

Microtremor observations were carried out for constructing a subsurface ground model in Palu. Array observations were conducted at 8 sites, which covered almost the whole city area. The dispersion curves of a Rayleigh wave were obtained from the data of array observations. The Kriging method can be used for the interpolation of subsurface information such as shear wave velocity and depth of irregular boundary. By conducting an inversion analysis for the calculation of dispersion curves, the subsurface structure beneath the site can be estimated. We constructed a four layered model in each array observation point. We reconstructed unified two-layered model by averaging the first three layers obtained from array observation. The shear wave velocity of the top layer is $Vs \leq 300$ m/s. By combining above two-layer model and the results of single point observation, we proposed the distribution of the first layer thickness of the sediment. Strong ground motions of the Palu area were predicted based on the stochastic Green's function method by using the proposed

ground model. Peak acceleration becomes more than 400 gal, peak velocity becomes more than 30 kine in some areas and peak ground displacement becomes more than 17 cm in some areas, which causes severe damage for buildings in high probability.

Acknowledgements

This study was supported by the Grant-in-Aid of JICA/SEED-Net. We gratefully acknowledge Dr. Noguchi and Dr. Ono in Tottori University for their cooperation with the microtremor observations and Dr Aiko Furukawa, Department of Urban Management, Graduate School of Engineering, Kyoto University for providing her invaluable support and encouragement during the research period in Kyoto. We sincerely thank Tadulako Universities for their help in undertaking the observations in Palu, Indonesia.

References

[1] B. Priadi.,(1993): Geochimie du magmatisme de l'Ouestet du Nord de Sulawesi, Indonesia:Tracage des sources et implications geodynamique. Doctoral thesis, Universite Paul Sabatier, Toulouse, France.

[2] ISC, (2007), *Historical Worldwide Earthquakes.* http://earthquake.isc

[3] S. Pramumijoyo., A. Setianto., W. Wilopo., P. S Thein.,(2012): The Steps to earthquake mitigation for Palu City, the Capital of Central Sulawesi Province, Indonesia. The 5th AUN/SEED-Net Regional Conference on Geodisaster Mitigation in Asean, Manila, Philippines.

[4] P.S.Thein, S. Pramumijoyo., K.S.Brotopuspito.,W. Wilopo., J.Kiyono and , A. Setianto (2013): To Estimates Sediment Thickness by Microtremor Single Station Measurements in Palu Area, Central Sulawesi, Indonesia, The 5th AUN/SEED-Net Regional Conference on Geological Engineering, Kuala Lumpur, Malaysia, ISBN: 978-967-0380-23-0, p.257

[5] P.S.Thein, S. Pramumijoyo., K.S.Brotopuspito.,W. Wilopo., J.Kiyono and , A. Setianto (2013): Estimation of Sediment Thickness by Using Microtremor Observations at Palu City, Indonesia, ASEAN ++ 2013 Moving Forward, The 11th International Conference on Mining, Materials and Petroleum Engineering, Chaing Mai, Thailand. p.52

[6] P.S.Thein, S. Pramumijoyo., K.S.Brotopuspito.,W. Wilopo., J.Kiyono and , A. Setianto (2013):Investigation of Subsurface Soil Structure by Microtremor Observation at Palu, Indonesia, The 6th ASEAN Civil Engineering Conference (ACEC) & ASEAN Environmental Engineering Conference (AEEC), Civil and Environmental Engineering for ASEAN Community, Bangok, Thailand,. p.C-6

[7] S. Pramumijoyo., S. Indarto., C. Widiwijayanti., and J. Sopaheluwakan. ,(1997): Seismic Parameters of the Palu-Koro Fault in Palu Depression Area, Central Sulawesi. Indonesia J. SE Asian Earth Sci.

[8]R.A.B. Soekamto.,(1995): Regional Geological Map of Palu Sheet, Indonesia, Scale 1:250,000, Geological Research Center, Bandung.

[9] K. Aki (1957): Space and time spectra of stationary stochastic waves, with special referent to microtremor, Bull. Earth. Res. Inst., Vol.35, No.3, pp.415-456.

[10] H. Nakagawa, H. Suzuki & H. Saito (2012): Extended CCA Method for Estimating Phase Velocity Using Arbitrarily Shaped Arrays, Geophysics, 15 WCEE LISBOA 2012. Pp.1-3

[11] J. Kiyono, Y. Ono, A.Sato, T. Noguchi and , Rusnardi, P. R. (2011): Estimation of subsurface structure based on Microtremor observations at Padang, Indonesia, ASEAN Engineering Journal, Vol.1, No.3, pp.66-81.

[12] J. Keneddy and R. C. Eberhart (1995): Particle swarm optimization, Proc. of IEEE International conference on Neural Networks, Vol.4, pp.1942-1948.

[13] T. Noguchi, T. Horio, M. Kubo, Y. Ono, J. Kiyono, T. Ikeda and Rusnardi P. R (2009), Estimation of Subsurface Structure in Padang, Indonesia by Using Microtremor Observation, Report on Earthquake Disaster Prevention Field, Tono Research Institute of Earthquake Science, Seq. No.26, pp.1-16, (in Japanese).
[14] J. Kiyono and M. Suzuki (1996): Conditional Simulation of Stochastic Waves by Using Kalman Filter and Kriging Techniques, Proc. of the 11th World Conference on Earthquake Engineering, Acapulco, Mexico, Paper No.1620.